INTEGRATED SIMULATION APPROACH FOR STRUCTURAL ANALYSIS OF COMPOSITE COMPONENTS CONSIDERING PROCESS SIMULATION DATA

N. Mayer[1], J. Prowe[2], T. Havar[2], R. Hinterhölzl[1] and K. Drechsler[1]

[1]Institute for Carbon Composites, Faculty of Mechanical Engineering, Technische Universität München, Boltzmannstraße 15, D-85748 Garching b. München, Germany
Email: mayer@lcc.mw.tum.de, Web Page: http://www.lcc.mw.tum.de
Email: hinterhoelzl@lcc.mw.tum.de
Email: drechsler@lcc.mw.tum.de

[2]Department of Structure Engineering, Production and Aeromechanics, AIRBUS Group Innovations, Robert-Koch-Straße 1, D-82024 Taufkirchen, Germany
Email: jens.prowe@airbus.com, Web Page: http://www.airbusgroup.com
Email: tamas.havar@airbus.com

Keywords: aerospace, structural finite element analysis, manufacturing process simulation, liquid composite moulding, mapping, testing

Abstract
The aim in this study is to include virtual manufacturing process data in the structural finite element analysis on a component level. The main challenge here is to provide an as-built, more realistic structural simulation for carbon fibre reinforced composites with strength and stiffness predictions based on discontinuous data from preceding manufacturing steps such as preforming and liquid composite moulding. This abstract describes the method developed for data conversion through mapping algorithms. Secondly, different approaches to consider shearing effects in stiffness prediction models such as the one of Halpin-Tsai for unidirectional lamina or a one-dimensional undulation model for woven fabrics, are analysed. Hence, an integrated simulation tool chain is defined starting at the preforming stage, in which the actual material orientation and ply thicknesses are retrieved from preforming simulation, and ending with an analysis of the structural behaviour under operational conditions. For demonstrating purposes, a component is developed. The component is made of an aerospace qualified carbon fibre reinforced epoxy. At the end, the impact of this as-built, more realistic structural simulation approach is discussed. This work is supported by the German Federal Ministry of Education and Research (BMBF) through the project MAI Design.

1. Introduction

In the analysis of structures with composite materials, process simulations are less integrated into structural simulations. The need of a manufacturing simulation chain for composite components is growing in the last years in the industry because of manufacturing costs and process time optimisation. The full-integrated virtual process chain is still a challenge for processes with high-perfomance materials due to multi-physic and multi-level simulation approaches. Some commercial software packages implemented stand-alone solutions for manufacturing steps. Following partintegrated process chain simulations and integrated process approaches were published in order to predict the behaviour of the composite component on the macroscopic level. Particularly, integrated process models consider the influence of manufacturing effects.

Excerpt from ISBN 978-3-00-053387-7

In the 1990s an integrated process model for liquid composite moulding (LCM) was introduced by Long et al. [1]. This approach was based on the processing and mechanical properties prediction with the shear effect [2]. The modelling system for LCM uses an existing kinematic drape model and a FE-based flow simulation. Bickerton et al. investigated draping and its effect on the mold filling process during manufacturing of a curved composite part [3]. Further publications by Endruweit et al. [4] consider advanced approaches for a permeability calculation based on kinematic draping simulation results. A coupled pre-forming/injection simulation of LCM processes was also presented by de Luca [5].
Recent publications [6, 7] show the big interest on a simulation chain for composite components in the industry. Different established methods are combined e.g. for a multi-level analysis of a resin transfer moulding (RTM) process chain for unidirectional fiber reinforced composite components [8, 9]. Hahn investigated flow simulations based on data from an experimental characterisation image analysis for NCF fabrics [10]. An integration of the image analysis results for a woven fabric into the material modeling tool WiseTex and a subsequent flow simulation in ANSYS was undertaken by Swery et al. [11]. Dix et al. integrated FE ESI PAM-Form draping results in an integrated approach for an RTM simulation [9]. This approach is based on a commercial mapping software and python scripting. Kärger et al. introduced a CAE chain for unidirectional fibre reinforced composite components [12]. This concept present an integration of draping results for the RTM simulation. However, consolidation simulations were not considered. For complex geometries mapping algorithms for a matching of real surface data with a simulation model are required. The interaction between manufacturing and simulation is also important for manufacturing process optimisation and structural performance e.g. of AFP processes [13]. Furthermore, the integration of real fiber orientation data after a preforming process is interesting for a quality control of produced components [14].

The aim of this paper is to demonstrate the simulation approach for structural analysis of composite components considering process simulation data on a component level. Achieved results by kinematic, FE-draping, RTM, curing and structural simulations are presented. The as-designed and as-built stiffness behaviour were analysed and validated with the three point bending test results.

2. Methods

The integrated simulation approach uses simulation data inside the virtual manufacturing chain for a prediction of material properties and therefore for as-built simulations. The virtual manufacturing chain is demonstrated schematicaly in Figure 1. For a data transfer between different simulation approaches and incompatible finite element meshes the developed mapping algorithm was applied. This algorithm is described in detail in [15, 16]. For permeability prediction the method presented in [17, 18] was used on the mesoscopic level and applied at the component level based on FE-based draping results. For a stiffness prediction models such as the one of Halpin-Tsai for unidirectional (UD) lamina or a one-dimensional undulation model for woven fabrics were used, whereby the Ishikawa et al. model was extended for sheared woven fabrics and is presented in [19]. This approach was applied for a calculation of engineering costants for curing and structural simulations with two different methods for the fibre volume content calculation (FVC): FVC1 according to [20] and FVC2 according to [18]. The strength prediction for woven fabrics at the component level was only possible with a representation of the woven fabric as a symmetrical lay-up of four UD plies. The following Section demonstrates the application of the developed methods on a generic geometry.

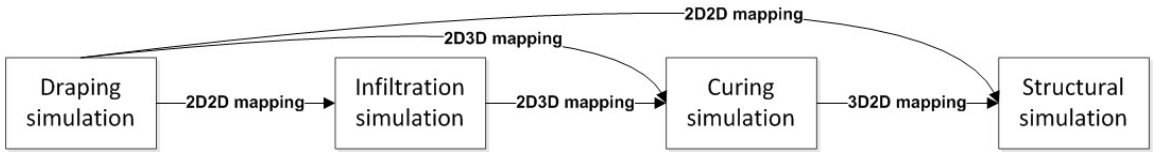

Figure 1. The virtual manufacturing chain up to the structural simulation.

Excerpt from ISBN 978-3-00-053387-7

3. Simulations

For the investigation of manufacturing effects on a component level and for a validation of structural simulation results a generic demonstrator geometry was designed. The geometry of the component is demonstrated in Figure 2. The manufacturing process steps were analysed by draping, infiltration and curing simulations. The demonstrator has been made of a HTA carbon fibre satin weave fabric and RTM6 epoxy resin with a lay-up of two [0°/90°] plies.

3.1. Kinematic and FE-based draping simulations

A draping simulation has been performed with different software packages: CATIA, DrapeIt, PAM-Quickform and PAM-Form. At first, kinematic simulations were considered for one ply of [0°/90°] woven fabric, where the start point was defined on the top of the geometry in the middle. In all kinematic simulations the distance between warp and weft yarns of 2 mm for the draping mesh was defined. For an FE-based stamping process the lay-up of two [0°/90°] woven fabrics was defined. The set-up of the stamping process was performed in PAM-CRASH. The plies of 350mm x 495mm were discretized into 175000 shell elements with an element edge of 1mm. Moulds (female and male), blankholder and table were discretized into triangle and shell elements with an average edge of 1mm. Mould and table were modeled with aluminium and the blankholder with steel materials. The female mould and the table was fixed in all directions (translation and rotation). For the male mould boundary conditions with one degree of freedom in z-direction and the velocity were defined. For the blankholder the boundary conditions with one degree of freedom in z-direction and the pressure were defined. All parts were defined as a rigid body with a center of gravity rigid body node (COG). The pressure of 3.55E-6 GPa was applied on the blankholder part.

Different solvers produced similar results for the kinematic simulation. The FE simulation output is strongly dependent on the input parameters and applied boundary conditions. It was observed, that the end results are close to the real process (see Section 4). However, one shear angle field at the last time step can not be calculated due to numerical problems. The simulation results at the next to the last time step included material waviness due to the not fully completed stamping process. At all simulations, the shear angles were overestimated in areas which are shown in Figure 2. A lower gradient of the stamp displacement with a high number of time steps can reduce but not eliminate this effect.

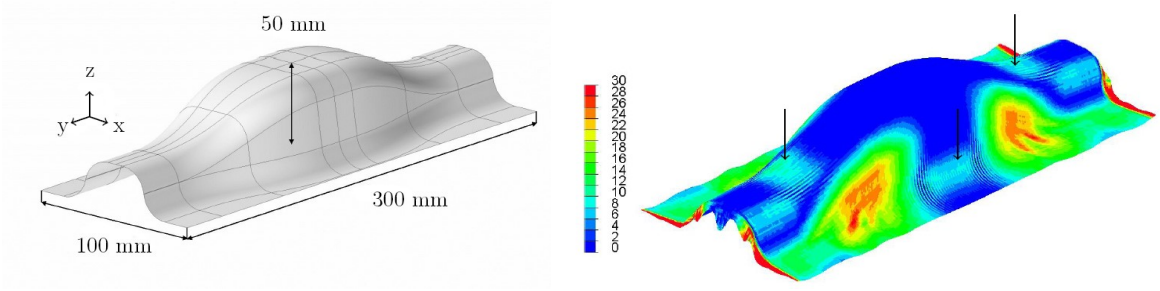

Figure 2. Geometry of the demonstrator (left) and FE-based draping results: shear angle (right).

.

The simulations were conducted on an Intel(R) Core(TM) i7-3740QM CPU 2.70GHz processor with 1 and 4 threads. Kinematic simulations are performed in seconds, CPU time for the FE-simulations is varied between 2.4102E+04 seconds for one ply and 1.118E+05 seconds for two plies with 25 time steps and 4 threads. With 300 time steps, the CPU time can increase up to 3.012E+05 seconds. The maximal shear angle for the 0°/90° fabric lies at 29.9° by Catia, 29.3° by PAM-Quickform, 29.3° by DrapeIt and 28.1° − 31.1° by PAM-Form softwares correspondingly.

Excerpt from ISBN 978-3-00-053387-7

3.2. Mapping of FE draping results

The developed mapping tool with 2D2D option was applied for a transfer of FE draping results onto an infiltration mesh. Mapping results are presented in Figure 3. A transfer of PAM-Form and PAM-Quickform results is also possible with the implemented mapping tool in the PAM-RTM software. However, it is difficult to influence these mapping results. The developed mapping tool with 2D3D option was applied for a transfer of FE-draping results onto the curing mesh. The developed mapping tool with 2D2D option was applied for a transfer of FE-draping fibre orientation and thickness distributions onto a structural mesh (see Figure 3).

PAM-RTM post processing was used for the illustration of the mapped shear angle fields. Due to a coarse infiltration mesh the mapping results are smoothed. It should be noted, that the draping results were used from the step where the distance between female and male mould was of 2 mm due to shear angle calculations problems (see Subsection 3.1). Therefore, the draping mesh represents the designed geometry not exactly (see Figure 3). This effect caused shear angle differences in some areas of the structural mesh.

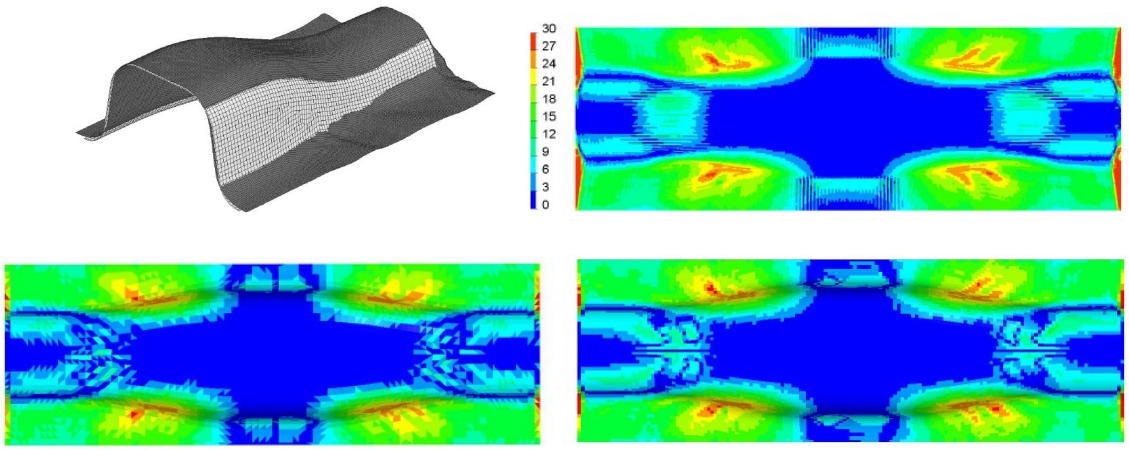

Figure 3. The source and target meshes (top left) and shear angle field on the source draping mesh (top right), the target infiltration mesh (bottom left) and the target structural mesh (bottom rigth).

3.3. RTM simulation

Infiltration simulations have been performed for an RTM process with the lay-up of [0°/90°] woven fabric. The permeability calculations were undertaken with the method published in [17,18] using FE draping results without a material variability. The values for the permeability of the used woven fabric with geometrical characteristics were presented in [21]. The maximal yarn fibre volume was assumed by 0.79 [22]. Therefore the initial layer fibre volume content according to [22] is 0.57. The ply was discretized in 5972 first order triangle shell elements with an average element edge of 3.3mm. As-designed and as-built simulations based on mapping results for fibre orientation fields were considered. For as-built simulations the first principal permeability directions were defined between warp and weft fibres dependent on positive and negative shear angle. An injection gate was defined on the right side of the mesh geometry. The simulations were calculated with the PAM-RTM solver 2014. Figure 4 shows simulation results for a [0°/90°] ply based on following configurations:

- AD: as-designed simulation.
- AB FE: as-built simulation based on PAM-Form results with a permeability prediction.

Excerpt from ISBN 978-3-00-053387-7

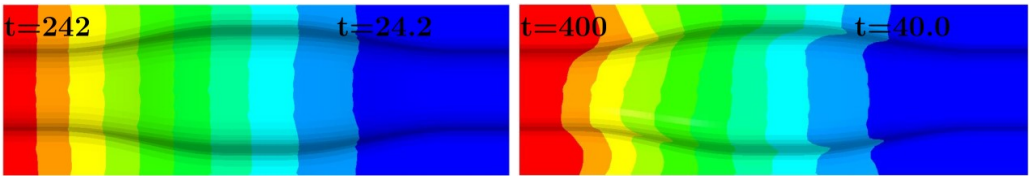

Figure 4. Infiltration simulation results for the [0°/90°] ply: AD (left) and AB FE (right).

.

3.4. Consolidation simulation

A consolidation process was simulated with a curing simulation based on a phenomenological approach with the ABAQUS solver 6.14-2. The curing simulation was defined with the temperature difference of 140°C (160°C-20°C). The demonstrator was analysed with a lay-up of two [0°/90°] plies where a mesh with 11729 solid (continuum) C3D20R elements was used for every ply with an element edge of 2 mm and thickness of 0.37 mm. As-designed simulation used a projected global coordinate system onto a middle surface of the solid elements. PAM-Form draping results were integrated into as-built simulations with the approach based on the stiffness modelling for woven fabrics (see Section 2) and the UD approach, where every fabric ply was represented by four plies inside one solid element. The effective thermal expansion coefficients were calculated with ESAComp software based on UD thermal expansion coefficients for a [0°/90°, 90°/0°] laminate. Poisson's ration values were estimated with ESAComp software based on material data for the HexPly 922-1 woven G926 nominal fabric. It should be noted, that the shearing effect influences both, stiffness properties and thermal expansion coefficient. In this work, as-built simulation with a smeared approach do not consider the influence on the effective thermal expansion. As-built simulation with an UD approach take into account the shearing influence due to the CLT. Figure 5 shows the influence of process fibre orientations onto the simulation results with the UD approach.

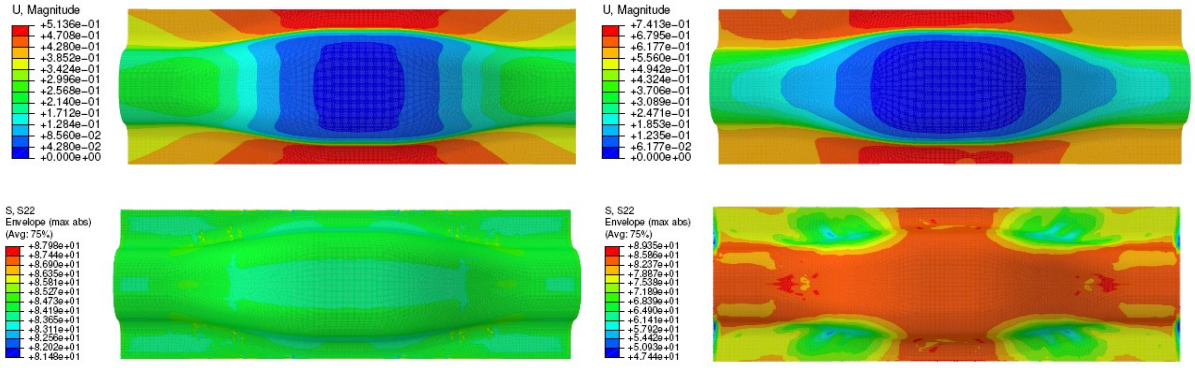

Figure 5. Displacement field $||u||_{max}$ for the lay-up of two plies: AD (top left) and AB FE (top right). Stress field s_{22} for the lay-up of two plies: AD (bottom left) and AB FE (bottom right).

.

3.5. Structural simulation

The static structural analysis has been performed with the ABAQUS solver 6.14-2. Three point and four point bending tests were conducted with different configurations based on as-designed material properties and with different composite lay-ups and load elements (elastic or non elastic). The focus was on a detection of maximum stressed areas of the component outside the load point concentrations. To avoid high stress concentrations and therefore local material damage, a contact surface between the load element and the testing part should be modeled with an appropriate size. Therefore, a rectangular load element was preferred instead of a cylindrical. The load element was discretized in linear C3D8I elements with an element edge of 2 mm and a Surface-to-Surface contact was used. Two supported

Excerpt from ISBN 978-3-00-053387-7

elements were modeled as rigid cylindrical bodies with a Node-to-Surface contact. Finite sliding formulation was used for both type of contacts. Figure 6 illustrated the used configuration for a three point bending test. The lay-up of two [0°/90°] plies was used where a mesh with 11729 shell elements (linear S4 elements with an average element edge of 2 mm) for every ply. A displacement of -1 mm was applied onto the load element. The friction coefficient of 0.25 between steel and composite material was applied [23]. A friction behaviour in tangential direction was modeled isotropic with Coulomb-Model [24]. However, due to a sliding behaviour of the demonstrator on the supported elements simulations with frictionless contacts were more appropriate to the real behaviour (see Section 4). Here, only results at -1mm displacement are presented.

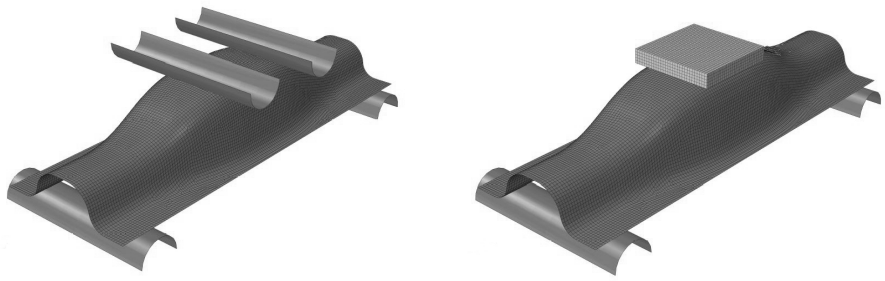

Figure 6. Four (left) and three (right) point bending test configurations.

Table 1 presents the stiffness evaluation for different configurations based on the load-displacement response. The load-displacement response was calculated with the accumulation of the z-component of the reaction force applied onto the nodes of the load element and displacement in z-direction. The element thickness t=0.37 mm was defined in AD 0.37 mm, AB FE FVC1 0.37 mm, AB FE FVC2 0.37 mm and AB K FVC1 0.37 mm structural models (FE = FE-based, K=kinematic draping results). The mapped element thickness were used in AB FE FVC1 T and AB FE FVC2 T models. By the stiffness modelling the mapped thickness values were used in AB FE FVC1 T and AB FE FVC2 T representative volume elements (RVEs). The difference between as-designed and as-built simulation results by a constant thickness ranges from 4.5% to 14.2%. The difference between AB FE FVC1 T and AB FE FVC2 T results is due to different calculation methods for FVC.

Table 1. Stiffness evaluation at -1 mm displacement.

Configuration	$\lvert F_{max} \rvert$ (N)	Deviation to AD 0.37 mm (%)
AD 0.37 mm	71.49	0.00
AB FE FVC1 0.37 mm	68.27	4.50
AB FE FVC1 T	62.87	13.70
AB K FVC1 0.37 mm	67.54	5.52
AB FE FVC2 0.37 mm	66.58	6.86
AB FE FVC2 T	61.31	14.23

4. Experimental work

For a validation of as-built structural behaviour, demonstrator components were manufactured and tested. The components were manufactured with the VAP process. Figure 7 demonstrates the VAP tooling with integrated heating elements used for the infiltration process with the RTM6 resin system. A matched-tool preforming process was realised with a hydraulic press and a preforming tooling,

Excerpt from ISBN 978-3-00-053387-7

where electrical heating elements were used for a binder activation. The binder Spunfab PA1203 [25] was used for preform stabilisation after the draping process. Figure 7 shows the developed male and female toolings with a blankholder (according to a draping simulation configuration).

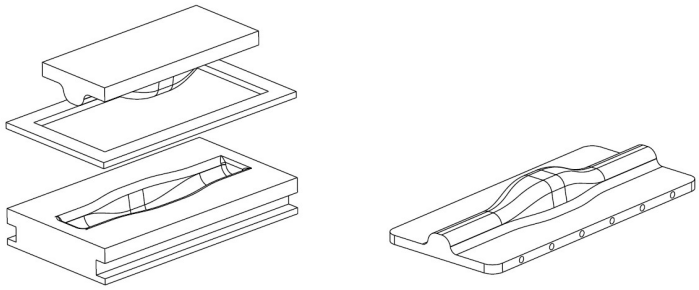

Figure 7. Preforming (left) and VAP (right) toolings.

4.1. Manufacturing

Two plies were prepared as a preform with a symmetrical lay-up of satin weave where one ply was mirrored. A binder was placed between the two plies. The draping process was performed with a hydraulic press (Hans Schoen GmbH) where the force-displacement values could not be measured. The male tooling was fixed on the top of the press stamp and pressed controlled by a force up to 100 kN and stamped inside the female tooling. The process temperature of the preforming tool during the process was 60°C and for the binder activation 115°C.

After the draping the preform was cut to a size of 360mm x 160 mm and infiltrated according to [26] at 120°C. A global FVC was calculated with the weight of the dry and the infiltrated preform. At the end all components were tempered at 180°C for 120 min. In total six components were manufactured for mechanical testing. The components were trimmed to a size of 300mm x 100mm at the *xy* plane according to the simulated component. The preform and the cured demonstrator parts are shown in Figure 8.

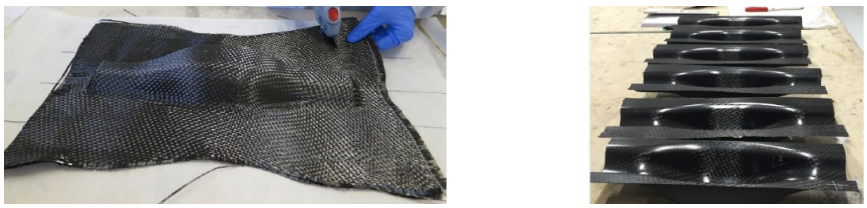

Figure 8. The preform (left) and the cured components (right).

4.2. Testing

A three point bending test was carried out with a HegewaldPeschke Inspekt Table100 universal testing machine with a 100kN load cell. The displacement was measured at the long side of the demonstrator with the 3D optical system ARAMIS. Also, biaxial strain gauges (Tokyo Sokki Kenkyujo Co.,Ltd.) were applied in critical areas predicted by the static structural analysis. All tests were conducted at a displacement rate of 2 mm/min at room temperature with T_average = 23°C. Displacement measurements were started with a trigger at 5 N and stopped at a displacement of -20 mm.

The displacement field measurement was undertaken by the testing machine and the ARAMIS system. ARAMIS cameras can produce some deviations due to the complex geometry. Therefore, ARAMIS

Excerpt from ISBN 978-3-00-053387-7

gave only a global overview of the structural behaviour. It was observed that the demonstrator displacement field is symmetrical. The load displacement response is demonstrated in Figure 9 based on values from the testing machine. The failure zone was detected on the flanges in the middle or close two the middle at -11 mm , -12 mm and -14 mm.

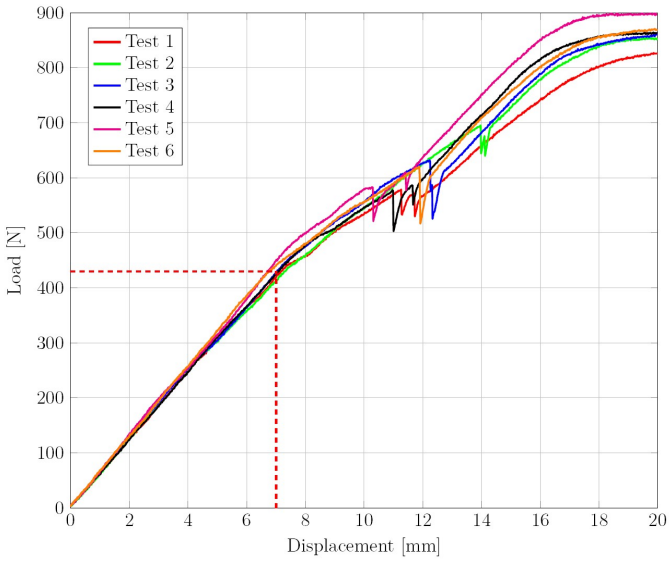

Figure 9. Load-displacement response for six test components.

The average testing load response at -1 mm displacement was observed by 60 N with a standard deviation of 3 N. Therefore, the achieved testing results are within a difference from 1% to 10% to as-built simulation results.

4. Conclusions

Detailed investigations of process and structural simulations based on the preforming process simulation data were undertaken on a generic geometry. In case of infiltration simulations impact of meso modelling on the component level was shown. In case of curing simulations the impact of fibre orientation effects is present by the UD modelling strategy. For more realistic curing simulations with the approach based on a woven fabric modelling besides mechanical properties predictions, an additional adaption of thermal expansion coefficients to process fibre orientations is needed.

Static structural simulations were undertaken with several configurations and validated with three-point bending tests. It was shown that as-built simulations can predict the stiffness behaviour close to the experimental results. FE-based and kinematic based as-built simulation results are similar due to the small shear angle on the flanges where the load concentrations are present.

The developed methods and the designed generic geometry can be used for further studies with different polymer composite materials and manufacturing processes.

Acknowledgments

This work was supported by MAI Carbon Cluster Excellence Initiative in the project MAI Design. We appreciate fruitful discussions and exchange on this topic with Prof. A. Long and Dr. A. Endruweit from the University of Nottingham, United Kingdom. Furthermore, we would like to thank our team colleagues and our students for the support.

Excerpt from ISBN 978-3-00-053387-7

References

[1] A. Long, P. Blanchard, C. Rudd, and P. Smith. The development of an integrated process model for liquid composite moulding. *Composites Part A: Applied Science and Manufacturing*, 29(7): 847–854, 1998.

[2] P. Smith, C. Rudd, and A. Long. The effect of shear deformation on the processing and mechanical properties of aligned reinforcements. *Composites Science and Technology*, 57:327–344, 1997

[3] S. Bickerton, P. Šimáček, S. E. Guglielmi, and S. G. Advani. Investigation of draping and its effects on the mold filling process during manufacturing of a compound curved composite part. *Composites Part A: Applied Science and Manufacturing*, 9-10:801–816, 1997.

[4] A. Endruweit, X. Zeng, and A. C. Long. Understanding variability in the permeability of non-crimp fabric composite reinforcements. *Non-crimp fabric composites*, S. Lomov, Ed. Cambrige: Woodhead Publishing Ltd, 2011, ch. 9, pp. 216–241.

[5] P. de Luca, Y. Benoit, J. Trochon, O. Morisot, and A. Pickett. Coupled preforming/injection simulation of liquid composites molding processes. *Proceedings of the SAMPE 2002 Conference, Long Beach, USA*, 2002.

[6] J. Fuhr, N. Feindler, and P. Middendorf. Virtual analysis of draping effects on stiffness and strength of ply-based composite structures. *Proceedings of the NAFEMS Seminar "Simulation of composites - a closed process chain?", Leipzig, Germany*, 2014.

[7] A. Bulla and F. Ehrhart. A holistic simulation driven composite design process. *Proceedings of the NAFEMS Seminar "Simulation of composites - a closed process chain?", Leipzig, Germany*, 2014.

[8] L. Kärger, F. Fritz, D. Magagnato, S. Galkin, A. Schön, A. Oeckerath, K. Wolf, and F. Henning. Development stage and application of a virtual process chain for RTM components. *Proceedings of the NAFEMS Seminar "Simulation of composites - a closed process chain?", Leipzig, Germany*, 2014.

[9] M. Dix, S. Bickerton, M. Tryfonifis, and R. Hinterhölzl. Consistent virtual CFRP process chain using a modular CAE interface. *Proceedings of the NAFEMS World Congress, Salzburg, Austria*, 2013.

[10] C. Hahn. A simulation approach of permeability prediction for RTM process simulation. *Ph.D. dissertation*, Technische Universität München, Munich, Germany, 2014

[11] E. Swery, R. Meier, S. Lomov, K. Drechsler, and P. Kelly. Predicting permeability based on flow simulations and textile modelling techniques: Comparison with experimental values and verification of FlowTex solver using ANSYS CFX. *Composite materials*, 0:1–15, 2015.

[12] L. Kärger, F. Fritz, D. Magagnato, S. Galkin, A. Schön, A. Oeckerath, K. Wolf, and F. Henning. Development and validation of a CAE chain for unidirectional fibre reinforced composite components. *Composite structures*, 132:350–358, 2015.

[13] H. Lang, A. C. Nogueira, M. Jürgens, E. Hombergsmeier, R. Hinterhölzl, and K. Drechsler. Investigation on the structural behavior of a metallically 3D-reinforced CFRP/CFRP joint using a variable search based on finite element analyzes. *Composite structures*, 139:199–209, 2016.

[14] F. Heieck, J. Fuhr, and P. Middendorf. Quality assessment of 2d braided composites with optical measurement techniques. *Proceedings of the 18th International Conference on Composite Structures, Lisbon, Portugal,* 2015.

[15] N. Mayer, R. Hinterhölzl, and J. Prowe. Finite element mapping for a structural analysis of composites. *Proceedings of the 16th European Conference on Composite Materials*, Seville, Spain, 2014.

Excerpt from ISBN 978-3-00-053387-7

[16] N. Mayer, B. Van Den Broucke, J. Prowe, T. Havar, and R. Hinterhölzl. Finite element mapping for incompatible FE meshes of composite structures. Submitted in *Advances in Engineering Software,* 2015.

[17] A. Endruweit, X. Zeng, and A. C. Long. Understanding variability in the permeability of non-crimp fabric composite reinforcements. *Non-crimp fabric composites*, S. Lomov, Ed. Cambrige: Woodhead Publishing Ltd, 2011, ch. 9, pp. 216–241.

[18] A. Endruweit, X. Zeng, and A. C. Long. Multiscale modeling of combined deterministic and stochastic fabric non- uniformity for realistic resin injection simulation. *Advanced Manufacturing: Polymer Composites Science*, 1:3–15, 2014.

[19] N. Mayer, J. Prowe, T. Havar, R. Hinterhölzl, and K. Drechsler. Structural analysis of composite components considering manufacturing effect. *Composite Structures*, 140(15):776 – 782, 2016.

[20] T. McBride and J. Chen. Unit-cell geometry in plain-weave fabrics during shear deformations. *Composites Science and Technology*, 57:345–351, 1997.

[21] A. Endruweit, P. McGregor, A. C. Long, and M. S. Johnson. Influence of the fabric architecture on the variations in experimentally determined in-plane permeability values. *Composites Science and Technology*, 66(11-12):1778–1792, 2006.

[22] A. Endruweit, F. Gommer, and A. C. Long. Stochastic analysis of fibre volume fraction and permeability in fibre bundles with random filament arrangement. *Composites Part A: Applied Science and Manufacturing*, 49:109–118, 2013.

[23] Z. Eliezer, C. Schulz, and J. Barlow. Friction and wear properties of an epoxy-steel system. *Wear*, 46(2):397–403, 1978.

[24] V. Acary, F. Cadoux, C. Lemaréchal, and J. Malick. A formulation of the linear discrete coulomb friction problem via convex optimization. *Journal of Applied Mathematics and Mechanics*, 91(2):155–175, 1983.

[25] Spunfab PA1203. *Technical data sheet*. Online under http://www.spunfab.com (last accessed 12.02.2016).

[26] HexFlow RTM6. *Technical data sheet*. Online under http://www.hexcel.com (last accessed 12.02.2016).

Excerpt from ISBN 978-3-00-053387-7